Biosensors and Bioelectronics 68 (2015) 500–507

Contents lists available at ScienceDirect

Biosensors and Bioelectronics

journal homepage: www.elsevier.com/locate/bios

SPAD aptasensor for the detection of circulating protein biomarkers

Laura Pasquardini [a,*], Lucio Pancheri [b], Cristina Potrich [a,c], Alessandro Ferri [d], Claudio Piemonte [d], Lorenzo Lunelli [a,c], Lucia Napione [e], Valentina Comunanza [e], Maria Alvaro [e], Lia Vanzetti [d], Federico Bussolino [e], Cecilia Pederzolli [a]

[a] Fondazione Bruno Kessler, Laboratory of Biomolecular Sequence and Structure Analysis for Health, via Sommarive 18, 38123 Povo (Trento), Italy
[b] DII -Department of Industrial Engineering, University of Trento, via Sommarive 9, 38123 Povo (Trento), Italy
[c] CNR-Institute of Biophysics, Unit at Trento, via alla Cascata 56, 38123 Povo (Trento), Italy
[d] Fondazione Bruno Kessler, Center for Materials and Microsystem (CMM), via Sommarive 18, 38123 Povo (Trento), Italy
[e] Department of Oncology, University of Torino and Institute for Cancer Research at Candiolo (IRCC), Strada Provinciale 142, 10060 Candiolo (Torino), Italy

ARTICLE INFO

Article history:
Received 31 October 2014
Received in revised form
8 January 2015
Accepted 19 January 2015
Available online 19 January 2015

Keywords:
Aptamer
VEGF
Chemiluminescence
SPAD

ABSTRACT

The need for decentralized clinical tests together with the concept of time and cost saving are pushing the development of portable, miniaturized, compact biosensors with diagnostic and prognostic purpose. Here, we propose an innovative detection system based on a Single Photon Avalanche Diode (SPAD) with high sensitivity and low noise, crucial features for an efficient chemiluminescence biosensor. The SPAD detector, having 60 μm diameter, has a Photon Detection Efficiency higher than 55% at 425 nm and a Dark Count Rate lower than 100 Hz at room temperature. Our design allows a good optical coupling efficiency between sample and detector. A specific biofunctional surface was implemented taking advantage of aptamers, short DNA sequences having high selectivity and affinity toward their targets. We successfully detected physiological levels of Vascular Endothelial Growth Factor (VEGF), a circulating protein biomarker highly correlated with cancer. The SPAD aptasensor showed a Limit of Detection (LoD) in the pM range, stability (up to 42 days) and re-usability (up to seven cycles). This compact biosensor is therefore a promising step toward the actual use of portable microdevices in diagnostics.

1. Introduction

Protein biomarkers are becoming increasingly significant tools from a clinical point of view not only in oncology, but also to guide for example the clinical treatment of infections (Huang et al., 2014). Panels of protein biomarkers have been indeed recently proposed as prognostic factors both from easily accessible biological fluids such as serum (Chung et al., 2014) and from tissues (Severi et al., 2014). Due to their significance and consolidated use in clinics, protein biomarkers are also an attractive target of miniaturized biosensor-based assays. Examples of biomarkers detected with biosensors are present in the literature, with detection methods based on surface plasmon resonance (Liu et al., 2012, Cho et al., 2012), electrochemistry (Palchetti and Mascini, 2012, Lee et al., 2009), optics (fluorescence) (Freeman et al., 2012, Wang et al., 2014), chemiluminescence (Zhang et al., 2014) or even label-free detection (Byeon and Bailey, 2011, Luchansky and Bailey, 2012, Pasquardini et al., 2013). Among the optical detection techniques, chemiluminescence is one of the most promising for the development of miniaturized biosensors due to the simple setup required, not requiring illumination sources neither long optical paths (Myers and Lee, 2008). Chemiluminescence systems require indeed two crucial elements: (i) a detector with high quantum efficiency and low noise and, (ii) a high optical coupling efficiency between sample and detector. To obtain these desirable features, chemiluminescence detectors are usually based on photomultiplier tubes (PMTs), which offer excellent performance in terms of dark count rate and detection efficiency. However, PMTs require high operation voltages and feature a large size, which conflict with the development of compact and portable biosensors. On the other hand, surface or near-surface chemiluminescence detection has been demonstrated on dedicated Complementary Metal Oxide-Semiconductor (CMOS) optical sensors chips (Eltoukhy et al., 2006, Baader et al., 2011, Esposito et al., 2012, Caputo et al., 2013). Using advanced signal filtering techniques, electronic noise could be reduced so that the detection limit is governed by photon Poisson noise (Eltoukhy et al., 2006). In this condition, the main limitation for detection noise is the detector dark signal. Alternatively, Poisson-noise limited operation is obtained with the use of Geiger-mode Avalanche Photodiodes, also known as Single-Photon Avalanche Diodes (SPADs) (Cova et al., 2004), or SPAD arrays. The first use of a SPAD for chemiluminescence detection

* Corresponding author.
E-mail address: pasqua@fbk.eu (L. Pasquardini).

http://dx.doi.org/10.1016/j.bios.2015.01.042
0956-5663/

dates back to 1995 (Isoshima et al., 1995), where the device was coupled to the sample through an optical fiber and cooled in liquid nitrogen. More recently, SPADs were used in bioluminescent bacterial bioreporter detection (Ramiz et al., 2008, Li et al., 2012). In spite of these few examples, no surface assays with SPAD detectors have been presented up to now.

In this context, the coupling of a SPAD detector to a surface-based chemiluminescence assay has the appealing potentiality to address the development of a rapid, efficient, portable and miniaturized diagnostic biosensor for the detection of meaningful biomarkers. Here we selected the Vascular Endothelial Growth Factor (VEGF) as a circulating protein biomarker to demonstrate the feasibility of this design. The VEGF family has indeed a crucial role in the angiogenesis event, which normally occurs during embryonic organ growth and development, or during reproduction or physiological repair in adults (Finley et al., 2011). However, angiogenesis (and therefore VEGF) has a crucial role also in pathological conditions where neovascularization is induced, favouring cancer development and growth and metastasis diffusion (Kut et al., 2007). Among the several isoforms exhibited by human VEGF (Zampros et al., 2012, Finley et al., 2011, Freeman et al., 2012), the predominant are VEGF165 and VEGF121, whose length is 165 and 121 amino acids, respectively. VEGF165 has a major role in angiogenesis (Kaur and Yung, 2012, Cho et al., 2012) and has therefore been selected as a privileged target in this study.

The VEGF level is usually detected by Enzyme-Linked ImmunoSorbent Assay (ELISA). Recently, however, other protein recognition systems based on aptamers have been proposed (Cho et al., 2012, Freeman et al., 2012, Lee et al., 2009, Liu et al., 2012, Palchetti and Mascini, 2012, Zhang et al., 2014, Wang et al., 2014). Aptamers are short single-stranded DNA or RNA molecules, or even peptides, having high selectivity and affinity toward their targets. Aptamers present many advantages over antibodies, such as high reproducibility in target recognition, easiness in being chemically modified and high stability even in non-physiological conditions (Song et al., 2008).

Here we propose a SPAD aptasensor, where a silicon oxide surface is coated by aptamers specific for the capturing of VEGF, which in turn is recognized by specific antibodies detected via chemiluminescence with a SPAD detector. Every step of aptasensor implementation was characterized both from the chemical and from the morphological point of view by using XPS and AFM, respectively. Moreover, the developed aptasensor was characterized in terms of stability in time and re-usability. The SPAD detector described in this study is produced in custom technology at the FBK fabrication facility in Trento (Pro et al., 2013). Compared to most commercial SPADs, which employ liquid nitrogen or Peltier cooling to reduce the Dark Count Rate (DCR), the technology used to fabricate our SPAD boasts a low DCR at room temperature thanks to the optimization of both gettering process and doping profiles (Pro et al., 2013). Moreover, we employed a compact configuration which allows to place the sample very near to the SPAD with a consistent increase in the solid angle of light collection. All these characteristics return in a small biosensor size that allows its easy integration in a portable microdevice with the huge advantages of an easy miniaturization, reduced complexity and costs. A comparison of performances reached with the developed SPAD aptasensor with a standard ELISA assay is also shown.

2. Materials and methods

2.1. Substrates and reagents

A silicon oxide layer 366 ± 5 nm deep was thermally grown by wet oxidation at 975 °C in O_2 atmosphere, starting from a $\langle 100 \rangle$ silicon wafer. The wafer was then cut in suitable small pieces. For tests with the SPAD detector, cover slips (VWR International LLC, Radnor, PA, USA) with 0.14 mm thickness and 10 mm diameter were utilized as a support. 3-mercaptopropyltrimethoxysilane (MPTMS, 99%) purchased from Gelest Ltd. (Maidstone, Kent, United Kingdom), was used without any further purification. Toluene anhydrous (99.8%), toluene, sodium hydroxide, urea, glycine, mercapto-hexanol (MP-HEX), purified VEGF165 (0.3 mg/ml), monoclonal anti-VEGF antibody produced in mouse, hydrochloric acid and all powders for buffered solutions were purchased from Sigma-Aldrich s.r.l. (Milan, Italy).

The aptamer utilized in this study was reported by Potty et al. (2009) as a truncated version of a DNA aptamer previously identified by Gold and Janjic (2004). This aptamer recognizes VEGF with a K_d equal to 0.9 nM. A di-thiol modification and ten thymines bases were introduced at the 5'end: 5'–HO–$(CH_2)_3$–S–S–$(CH_2)_3$–T TTT TTT TTT CC CGT CTT CCA GAC AAG AGT GCA GGG -3'. The sequence is HPLC purified and was purchased from IDT Integrated DNA Technologies (Leuven, Belgium).

Goat anti-mouse IgG HRP-conjugated and blotto powder (non-fat dry milk) were purchased from Santa Cruz Biotechnology Inc. (Heidelberg, Germany). SuperSignal West Femto Chemiluminescent Substrate was purchased from Thermo Scientific (Rockford, IL USA).

2.1.1. Biological samples

EDTA-anticoagulated human blood from healthy donors was kindly provided by the Immunohematology Department, S. Chiara Hospital (Trento, IT). Plasma samples were obtained by centrifugation of whole blood at 700 g for 10 min and stored at –20 °C until use.

2.1.2. Albumin/IgG-depleted plasma and ELISA quantification

Plasma was processed for the removal of albumin and immunoglobulins G (IgGs) using PureProteome Albumin/IgG Depletion System (Millipore), according to the manufacturer's instructions. Briefly, plasma samples were diluted and incubated with PureProteome magnetic beads which provide a rapid and scalable means to deplete more than 90% of albumin and IgG from plasma samples; after recovery of albumin/IgGs depleted plasma, the resulting samples were concentrated to restore the initial sample volume. Albumin/IgGs depleted plasma and whole plasma were analyzed using Quantikine ELISA Human VEGF Immunoassay (R&D Systems) according to manufacturer instructions.

2.2. Methods

The procedure of the biosensor development is illustrated in Fig. 1.

In order to introduce thiol groups able to react with the 5' dithiol groups of the modified aptamer, the silicon oxide surface was functionalized in wet conditions with MPTMS, as previously described (Pasquardini et al., 2013). Briefly, SiO_2 substrates were cleaned with an argon plasma (6.8 W, one minute) to remove organic contaminants and to hydroxylate the surface and were then immersed in a 1% v/v solution of MPTMS in toluene anhydrous at 60 °C for 10 min. Silane-coated substrates were rinsed several times with toluene and then dried in a stream of nitrogen. 10 μM DNA–aptamer unfolded by thermal shock (95 °C, 1 min, ice for 10 min) and dissolved in Na_2CO_3/$NaHCO_3$ 0.5 M, pH=9 were added to mercaptosilanized surfaces for two hours on a slow orbital shaker. After a washing step, the surfaces were incubated with 1 mM mercapto-hexanol in the same buffer, in order to block the un-reacted free thiol groups on the surface. Three washing steps in buffer were performed to remove any passivating residues, leaving the aptamer-functionalized surface ready for the protein capture.

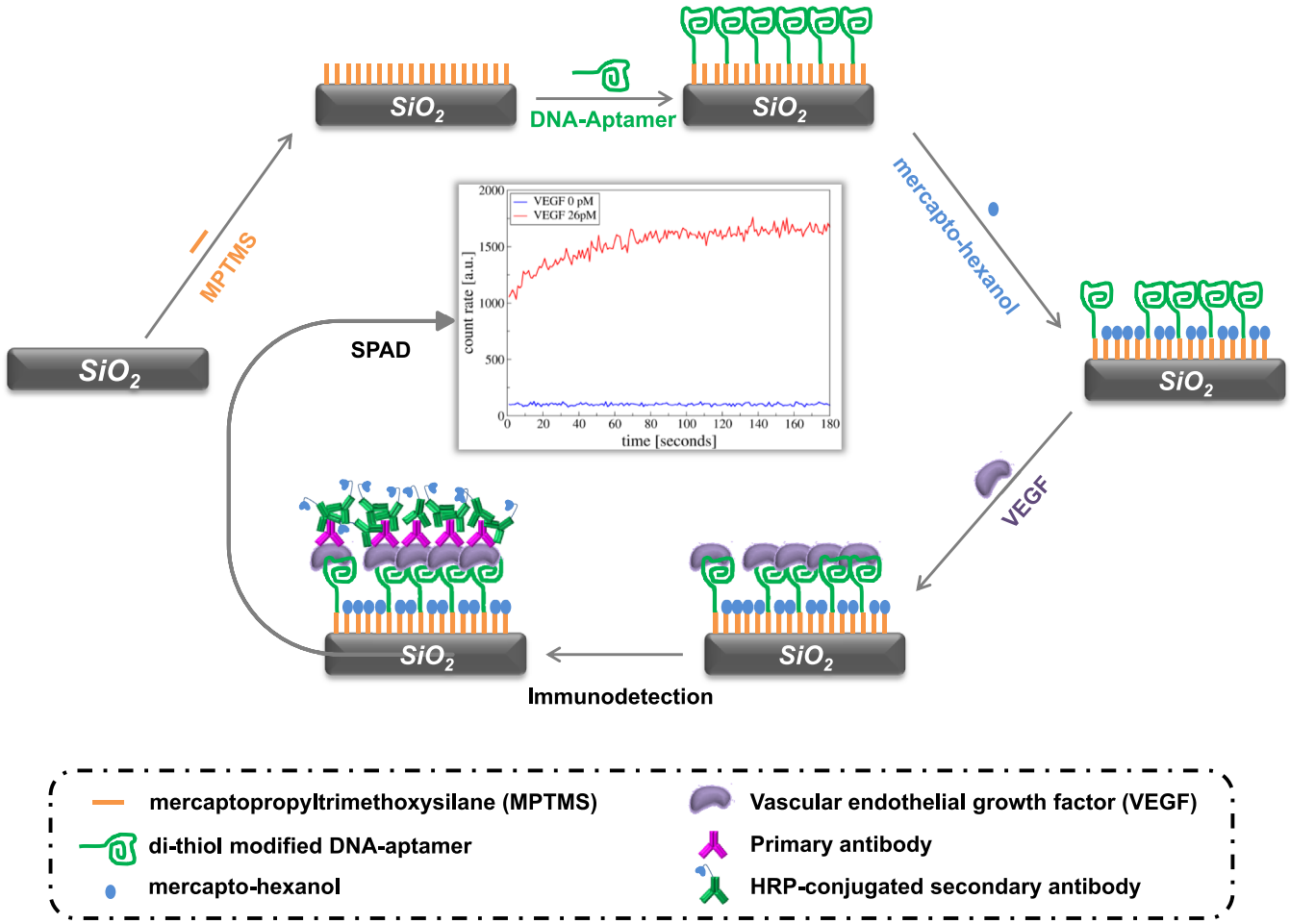

Fig. 1. Scheme of the SPAD aptasensor highlighting the different steps of the VEGF detection.

Different concentration of VEGF in 20 mM Tris–HCl pH 7.4 in the range 0/23,875 pg/ml were incubated on the surfaces. Experiments with human plasma were performed with 30% or 50% v/v human plasma diluted in the previous buffer or with undiluted plasma. After 1 h incubation and a washing step in buffer, the surfaces were passivated for 30 min in 3% blotto solution. The incubation with primary antibody was carried out in 3% blotto at 2 μg/ml for 30 min, followed by three washing steps to remove the excess of antibodies. The surfaces were then incubated with an anti-mouse IgG HRP-conjugated at 0.05 μg/ml in 3% v/v blotto, removing the excess of antibodies with three washes in buffer. Finally, the chemiluminescence signal was developed with the SuperSignal West Femto Chemiluminescent Substrate kit according to the manufacturer instructions, and detected using the SPAD detector as reported in Section 2.4 or a standard imaging system (Gel-Logic 1500 detection system, Eastman Kodak Company), acquiring the signal for 1 min. Signal measured with the standard imaging system was quantified using the ImageJ software (Schneider et al., 2012).

2.3. Surface characterization

X-ray Photoelectron Spectroscopy (XPS) measurements were performed using a Scienta ESCA200 instrument equipped with a hemispherical analyzer and a monochromatic AlKα (1486.6 eV) X-ray source, in transmission mode. The emission angles between the analyzer axis and the sample surface was 15°, corresponding to a sampling depth of approximately 2–3 nm (Li et al., 2006). For each sample Si2p, O1s, C1s, and S2p core lines were recorded at a pass energy of 150 eV, with an energy resolution of 0.4 eV, using the low electron energy flood gun to compensate sample charging. The quantification, reported as relative elemental percentage, was done by using the integrated area of the fitted core lines, after Shirley background subtraction, and by correcting for the atomic sensitivity factors. This procedure gives a semiquantitative analysis allowing the surface chemical characterization at different modification steps. AFM measurements were performed using a Cypher AFM (Asylum Research, Santa Barbara, CA) in AC mode in air. AC240 silicon cantilevers (Olympus) with a nominal force constant of 2 N/m were used, acquiring images of different areas, ranging from 500×500 to 5000×5000 nm^2. Data were analyzed with Gwyddion (Nečas and Klapetek, 2012), applying a line-by-line levelling algorithm.

2.4. SPAD detector

SPAD detectors were fabricated in FBK using a dedicated technology (Pro et al., 2013). The SPADs have a peak Photon Detection Efficiency higher than 55% at 425 nm, well suited to the luminol light emission band (Pro et al., 2013). A sample device having a circular active area of 60 μm diameter and a DCR lower than 100 counts per s at room temperature was selected to conduct the experiments (see micrograph in Fig. 3A). The SPAD detector was glued and wire-bonded on a Printed-Circuit Board, and the bonding wires were protected with an epoxy resin. The SPAD detector, having an integrated polysilicon quenching resistance, was coupled to a low-noise high-speed comparator circuit for signal digitization. A 24-bit counter was directly connected to the

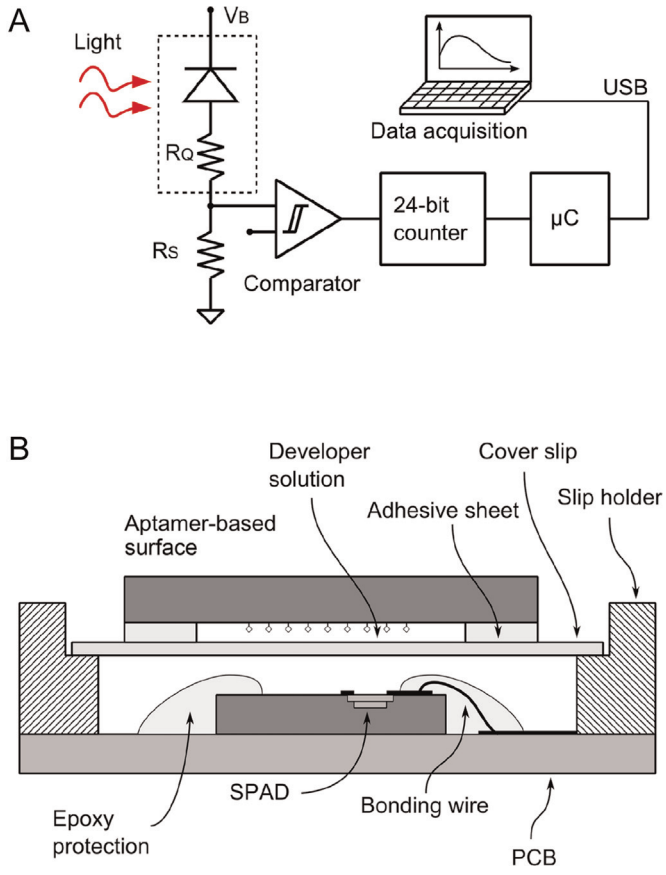

Fig. 2 (A) Block diagram of the detection system. (B) Schematic cross-section of the SPAD aptasensor. The aptamer-based surface carrying VEGF and antibodies is placed in close constant distance from the SPAD detector, which measures the chemiluminescence signal appearing when the developer solution is added.

comparator output to measure the count rate from the digital stream, and a PC was used for data logging (see Fig. 2A). The simplicity of the readout circuit is well suited for a parallel implementation in a low-cost application specific integrated circuit (ASIC). The experiments were performed placing the aptamer-based surface on a 140 μm thick cover slip directly on the top of the detector (Fig. 2B). A holder was used to keep the cover slip at 200 μm constant distance from the SPAD. Between the cover slip and the aptamer-based surface, positioned upside down, a 0.4 μl chamber was produced with a 120 μm thick adhesive sheet carrying a central hole of 2.5 mm diameter, where the development solution is added. The chemiluminescence signal was recorded by the SPAD (Fig. 2B) placed at a distance lower than 0.5 mm from the aptamer-based surface, ensuring a high light collection efficiency without the need of complex focusing systems.

3. Results and discussion

Here we explore a new design of a chemiluminescence biosensor for the detection of circulating protein biomarkers. A compact and portable SPAD with very high quantum efficiency and low dark count was coupled to an aptamer-based surface for the specific detection of VEGF, a well-known oncological biomarker. The performances of the aptamer-based surface were tested in terms of specificity, stability and reusability, while the innovative biosensor was tested with biologically relevant samples and compared with the standard ELISA assay.

3.1. SPAD signal-to-noise ratio and detection limit

The SPAD detector tested in this study has a circular active area with 60 μm diameter (Fig. 3A). The SPAD detection limit is uniquely determined by Photon Detection Efficiency (PDE) and DCR quantum noise, both depending on the applied voltage.

In an interval of time ΔT, the number of electrical output pulses C_{out} from the SPAD detector is proportional to the rate of incident photons N_{ph} through the equation

$$C_{out} = C_{chem} + C_{dark} = (PDE\ N_{ph} + DCR)\Delta T \quad (1)$$

where the useful signal is represented by the first term and the dark signal by the second term. At the low light levels expected for chemiluminescence, background subtraction is necessary to remove the offset due to DCR. An additional measurement has to be performed to acquire the dark count during the time interval ΔT and DCR is subtracted from the raw signal (C_{out}). Since both photogenerated and dark events follow Poisson statistics, the standard deviation of the corrected signal is given by

$$\sigma = \left[\left(PDE\ N_{ph} + 2DCR\right)\Delta T\right] \quad (2)$$

where the contribution of dark noise appears twice due to dark count subtraction. The Signal-To-Noise ratio can therefore be expressed by

$$SNR = C_{chem}/\sigma \quad (3)$$

The relative dependence of PDE and DCR at room temperature was measured using a blue LED light source, obtaining a DCR lower than 80 Hz. In the considered range, a linear relationship is observed between PDE and DCR (Fig. 3B). Remarkably, the dark count rate corresponding to the maximum PDE, corresponds to a primary dark current of 0.45 pA/cm^2, comparable to State-of-The art scientific CCD detectors (Janesick, 2001). The reported SPAD detector lacks the spatial resolution provided by CCDs, but provides pure Shot noise-limited operation. The SNR corresponding to the maximum PDE is plotted as a function of N_{ph} in Fig. 3C for different values of measurement time.

Considering a signal of 3σ ($SNR=3$), which allows a good discrimination of detected photons from DCR quantum noise, a detection limit of 6.7 photons/s ($\lambda=425$ nm) incident on the SPAD surface, corresponding to an irradiance of 1.1 nW/m^2, is obtained for 100 s exposure.

3.2. Implementation of the aptamer-based surfaces for biomarkers detection

The SPAD biosensor performances were tested detecting a well-known oncological biomarker (VEGF). A smart surface was implemented in order to achieve the specific capture of VEGF, as well as to fulfill the requirements of re-usability and stability typical of an integrated miniaturized biosensor. Aptamers were selected as capturing agents for their intrinsic properties of high reproducibility in target recognition, easiness in being chemically modified and high stability even in non-physiological conditions (Song et al., 2008).

Each step in the preparation of the aptamer-based surface (Fig. 1) was chemically and morphologically characterized via XPS and AFM, respectively. XPS core lines and AFM images are reported in Figs. S1 and S2 of Supplementary Information (SI). Table 1 shows the surface elemental compositions measured with XPS of the unmodified ("untreated" and "plasma-cleaned" surfaces) or mercapto-silanized silicon oxide substrates ("silanized" surface). From the comparison of the elemental composition before (surface "untreated", Table 1) and after the plasma treatment

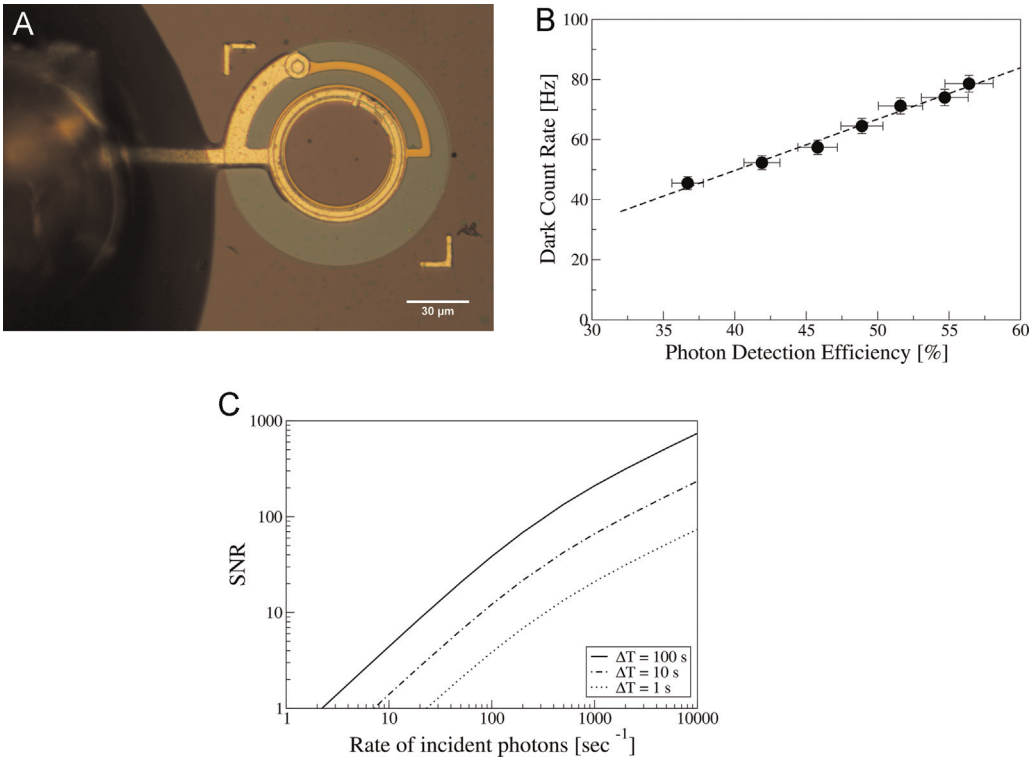

Fig.. 3 (A) Micrograph of the SPAD detector with 60 μm diameter. (B) Performance evaluation of the SPAD detector: Dark Count Rate as a function of Photon Detection Efficiency (λ=425 nm). Measurements are performed at room temperature (22 °C). Standard deviations are also reported. (C) SNR as a function of incident photon rate at 3 different integration times (1, 10, 100 s).

Table 1
Elemental composition (atomic percentage) determined by XPS analysis at 15° take-off angle after the different steps of surface functionalization. The standard error does not exceed the 1–2% of the reported value.

	O 1s (%)	C 1s (%)	Si 2p (%)	S 2p (%)
Untreated	38.8	30.7	30.5	–
Plasma-cleaned	54.3	8.6	37.1	–
Silanized	36.3	30.4	29.2	4.1

("plasma-cleaned", Table 1), a significant decrease in the carbon content is evident, confirming the effectiveness of the cleaning protocol. Moreover, the presence of silane molecules on the silicon surface was confirmed by an increase in the carbon content ("silanized", Table 1) with respect to "plasma-cleaned" surface. This increment, together with the presence of a sulfur peak, can be ascribed to the silane aliphatic chains and therefore to the actual silane coating. The chemical composition after the silane immobilization was indeed in good agreement with the literature (Lenigk et al., 2001, Zuo and Torres, 2010).

The morphology of the surface before and after silanization was also characterized. The roughness values R_a of the plasma-cleaned surfaces measured via AFM was 0.2 nm and changed only slightly after silanization. The change in the R_a values was in fact around 0.1 nm, in good agreement with Phaner-Goutorbe et al. (2011), suggesting that an homogeneous coating of the surface was achieved. On the contrary, after the binding of aptamers, the surface roughness increased to 0.6 ± 0.1 nm. This further small increment (0.3 nm), however, suggests that the silane layer was uniformly coated by aptamers. The subsequent passivation step decreased the little difference introduced by the aptamer deposition (0.5 ± 0.1 nm), as expected when the small passivating molecules fill the gaps in the aptamer layer. Finally, the roughness value after the VEGF capture was the same as after the passivation step, witnessing an uniform binding of VEGF to aptamers.

The results of the chemical and morphological characterization clearly lead to the conclusion that an uniform silane layer was successfully immobilized, allowing the subsequent efficient immobilization of aptamers. The following passivation step resulted in a smooth, uniform surface, suitable for the homogeneous capture of VEGF.

The aptasensor development was further characterized by binding the same anti-VEGF aptamer but conjugated with a fluorescent dye in order to assess the specificity of this binding (Figure S5, panel A). The binding was found to be specific for the silanized surface, while was negligible on bare silicon oxide. The VEGF detection was also proven by immunofluorescence (Figure S5, panel B).

3.3. VEGF detection with the SPAD aptasensor

Once characterized, the aptamer-based surface was placed very close to the SPAD detector (see Fig. 2B) and the performances of the biosensor were tested quantifying the VEGF content in different biological samples. A chemiluminescence signal was obtained adding a specific anti-VEGF antibody recognized by a secondary antibody HRP-conjugated (see Fig. 1 for details). HRP in the presence of hydrogen peroxide catalizes the oxidation of the substrate luminol (5-amino-2,3-dihydrophthalazine-1,4-dione) to 3-aminophthalate (Figure S3). This product decays from its excited state to a lower energy state by releasing a photon. The number of photons is in our conditions proportional to the number of HRP (and therefore to the number of VEGF molecules on the surface). These photons, taking in to account opportune efficiency factors, are then collected and counted by the SPAD detector. The SPAD count rate was recorded integrating the signal for one minute and the result was corrected for the dark count contribution. The recording started after few minutes of incubation of aptasensor and

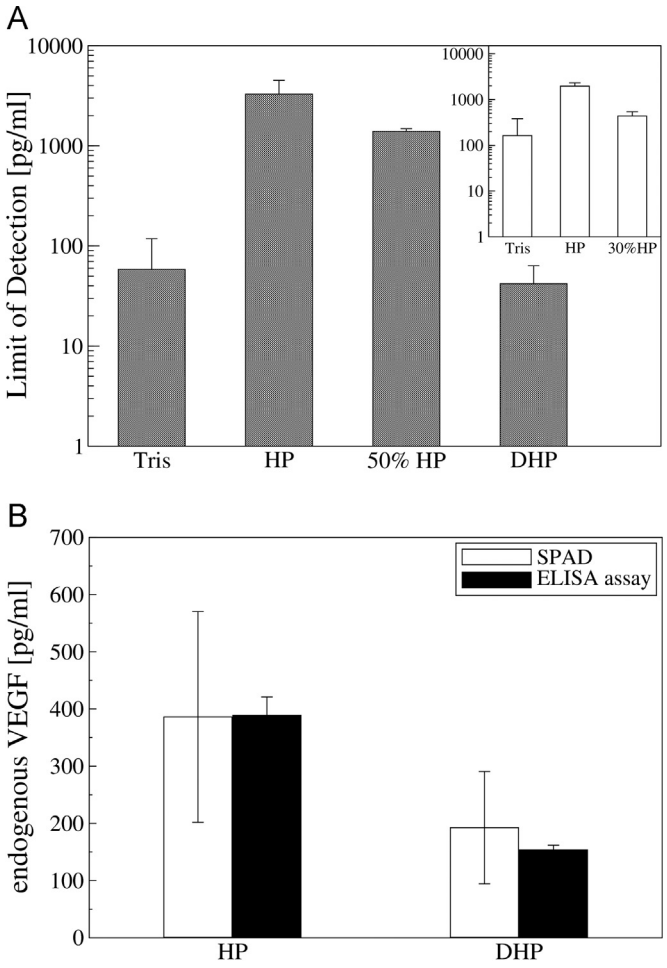

Fig. 4. Performance of the SPAD biosensor. (A) Limit of detection expressed as concentration (pg/ml) of VEGF spiked in buffer (Tris), in whole human plasma (HP), in 50% v/v human plasma diluted in buffer (50% HP), or in human plasma depleted from albumin and IgGs (DHP). Inset: LoD of same samples measured with a standard imaging system. Standard deviations are also reported. (B) Comparison of detection performances between the SPAD biosensor and a standard ELISA assay. Data are mean of three independent experiments.

the developing solution to let the chemiluminescence reaction reach its plateau (Fig. S6). In order to quantify the VEGF content a calibration curve was initially measured adding known amounts of VEGF spanning a range from 0 (pure buffer) to 10,000 pg/ml (Fig. S4). This curve was used for the quantification of VEGF in human plasma and in plasma depleted of albumin and IgGs, the most abundant proteins present in plasma and serum (Fig. 4A). The Limit of Detection (LoD) of the SPAD aptasensor in Tris buffer resulted 58 pg/ml, almost 3 times lower than that detected with a standard imaging system in the same conditions (Gel-Logic 1500 by Kodak, LoD 164 pg/ml, Fig. 4A inset), suggesting the use of the SPAD biosensor for biomarkers detection as very promising. Furthermore, the LoD measured in human plasma spiked with VEGF (1,715 pg/ml) is in the same range as the LoD measured with the standard imaging system (1,963 pg/ml). VEGF was also measured in diluted human plasma (50% HP, Fig. 4A), since these samples are routinely diluted by a factor two when measured with ELISA. The LoD measured in 50% HP samples (730 pg/ml) was halved with respect to the HP samples, but still higher than in buffer. The difference with buffer could be ascribed to the presence of highly abundant proteins in plasma which can compete with or limit the binding of low abundant biomarkers, such as VEGF. To verify this hypothesis, we measured a human plasma sample depleted from human albumin and IgGs (DHP, Fig. 4A). In this case, a LoD comparable to those of buffer was obtained, confirming the interference of highly abundant proteins in the binding of VEGF.

In addition to plasma samples spiked with VEGF, we quantified also the endogenous VEGF physiologically present in human plasma (three biological replicates, i.e. three plasma samples deriving from different individuals). Results were then compared to a standard quantification via ELISA (Fig. 4B). A good correlation between the two assays was found both for non-diluted human plasma and for the depleted plasma. Data acquired with the SPAD, however, are affected by larger errors with respect to ELISA (Fig. 4B). Both the smaller reaction volume and active area of the SPAD detector with respect to the standard ELISA concur to reduce the data reproducibility. Despite these disadvantages, the obtained results suggest that an improved aptasensor with an increased area of detection or with multiple SPAD sensors could reach the high stability and reproducibility required for biomarker quantification.

The amount of VEGF measured with both assays (Fig. 4B), however, is higher than that reported by Jelkmann (2001), i.e. 9–150 pg/ml VEGF in plasma from healthy donors. Nevertheless, this difference could be referred to a different procedure in sample handling, which can affect the overall protein quantification, as reported in the same paper (Jelkmann, 2001).

The LoD reached with our SPAD aptasensor for the quantification of VEGF in simplified solutions (i.e. about 60 pg/ml for Tris and DHP, Fig. 4A) is quite close to the declared sensitivity for a standard ELISA assay (i.e. 5–10 pg/ml). Notably, this result has been obtained with a volume of developer solution 250 times lower than with a standard imaging system. However, an increased sensitivity is still desirable in order to measure physiological VEGF levels in plasma. A lower LoD could be reached with our biosensor implementing for instance an optimized fluidic cell with low evaporation rate, which allows a longer integration time. Moreover, it is worth noting that the proposed configuration has the two-fold advantage of very simple sample-detector alignment and detector reusability. Further improvement of light detection efficiency can be obtained either by reducing the overall stack thickness, or by performing the detection directly on the SPAD detector surface. In this last case, however, packaging would become more critical and the detector itself should be disposable.

3.4. *Regeneration and stability of the aptamer-based surface*

After completion of VEGF detection, proteins (both antibodies and VEGF) on the surface can be removed using regeneration solutions, therefore making the functionalized surface reusable. The re-usability of the aptamer surface is indeed a crucial parameter when implementing a biosensor. Different regeneration solutions were tested: 50 mM NaOH, mixture of 50 mM NaOH and isopropylic alcohol (3/2 v/v), chaotropic agents (8 M urea), acidic solutions, but the best results were obtained with the acidic solutions (i.e. 50 mM HCl, 100 mM HCl, 100 mM glycine pH 2, Fig. 5A), according to the literature (Chen et al., 2010, Zhao et al., 2014). These solutions could perturb the protein tridimensional conformation, leading to unfolding or even degradation of proteins, which turn in freeing aptamers on the surface. After regeneration, new VEGF is incubated on the same surface and detected via chemiluminescence. Subsequent cycles of regeneration–incubation were performed to check the maximum number of regeneration cycles possible before substantially loosing the biosensor performances (Fig. 5A). The regeneration with 50 or 100 mM HCl or 100 mM glycine pH 2 gave similar results, inducing a decrease in efficiency that drops below 10% after 11 cycles. The efficiency of the aptamer-based surface remains still near to 50% of the initial value (dashed line, Fig. 5A) up to seven regeneration cycles.

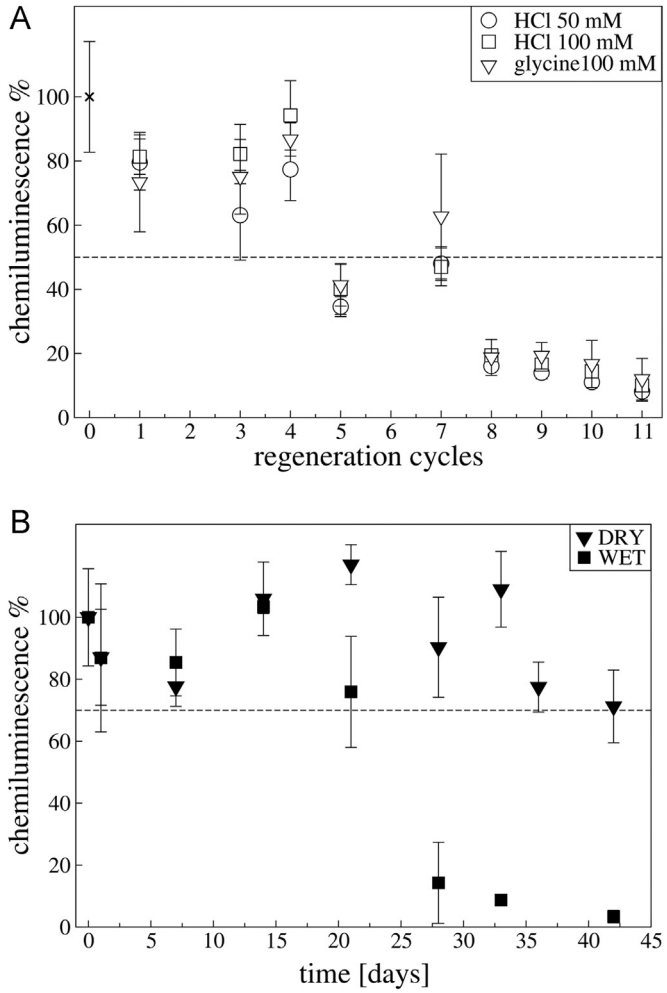

Fig.. 5 (A) Effect of regeneration cycles in different solutions: HCl 50 mM (open circles), HCl 100 mM (open squares) or glycine 100 mM at pH 2 (open down triangles). A cross mark indicates the chemiluminescence value obtained on the samples before the regeneration treatments. A dashed line is drawn to indicate a drop in efficiency of 50%. Data are mean of four independent experiments. (B) Chemiluminescence signal from 19,100 pg/ml of VEGF incubated on aged surfaces, preserved at 4 °C in air (DRY, closed down triangles) or buffer (WET, closed squares). The signal, normalized to the freshly-prepared surface, is the mean of four independent measures. A dashed line is drawn at 70% efficiency, dividing samples in two groups: those that maintain similar performances in time (upper region) from those that show a severe loss of performances (lower region).

The developed aptamer-based surface was also characterized in terms of stability in time. Replicas of the aptamer-based surface were preserved at 4 °C in air or in buffer for a time-course up to 42 days. At the desired time, VEGF was incubated on the surfaces and detected via chemiluminescence. The aptamer-based surfaces aged either in air or in buffer for up to 20 days showed similar performances to the freshly-prepared surfaces (Fig. 5B, values above the dashed line). Notably, after 42 days surfaces preserved in air maintain their detection performances, indicating that the dry preservation is the optimal packaging condition for the SPAD aptasensor.

4. Conclusions

The work here presented prove the feasibility to implement a sensitive, miniaturized, reusable chemiluminescence aptasensor, which can be a valid alternative to traditional assays for biomedical applications, such as the detection of circulating oncological biomarkers. The implementation of an aptamer-based surface for the specific capture of VEGF was characterized step by step from the chemical and morphological point of view, finding an uniform layer of aptamers distributed on the surface. The VEGF captured by the aptamer-based surface was detected in chemiluminescence with a SPAD detector, having the advantage of Poisson-noise limited operation, high PDE and low DCR. The detector was operated at room temperature, the optimal condition for the HRP reaction. The sensitivity of the SPAD aptasensor was proven in the same range as with standard imaging systems or ELISA, while the aptamer-based surface was stable up to forty-two days in dry conditions and reusable up to seven times when regenerated with acidic solutions. These performances could be further improved by optimizing the fluidic module and the packaging, resulting in a possible implementation of a compact, portable and integrated biosensor for the detection of circulating biomarkers.

Acknowledgements

This work was accomplished in the framework of the NAoMI Project (NAno-on-MIcro), funded by the Province of Trento “Grandi Progetti” No. 2790. The authors gratefully acknowledge Dr. Gina Rossetti and Mauro Waldner (Immunohematology Department, S. Chiara Hospital, Trento, IT) for providing human plasma samples and Cristian Collini (FBK-CMM, Trento, IT) for providing silicon oxide samples.

Appendix A. Supplementary material

Supplementary data associated with this article can be found in the online version at http://dx.doi.org/10.1016/j.bios.2014.05.063.

References

Baader, J., Klapproth, H., Bednar, S., Brandstetter, T., Rühe, J., Lehmann, M., Freund, I., 2011. Biosens. Bioelectron. 26 (5), 1839–1846.
Byeon, Ji-Y., Bailey, R.C.B., 2011. Analyst 136, 3430–3433.
Caputo, D., Nardini, M., Scipinotti, R., de Cesare, G., Mirasoli, M., Zangheri, M., Roda, A., Nascetti, A., 2013. Proc. SPIE 8774, 87740W.
Chen, W., Lei, Y., Li, C.M., 2010. Electroanalysis 22 (10), 1078–1083.
Cho, H., Yeh, E.-C., Sinha, R., Laurence, T.A., Bearinger, J.P., Lee, L.P., 2012. ACS Nano 6 (9), 7607–7614.
Chung, L., Moore, K., Phillips, L., Boyle, F.M., Marsh, D.J., Baxter, R.C., 2014. Breast Cancer Res. 16 (3), R63.
Cova, S., Ghioni, M., Lotito, A., Rech, I., Zappa, F., 2004. J. Mod. Opt. 51, 1267–1288.
Eltoukhy, H., Salama, K., Gamal, A.E., 2006. IEEE J. Solid-State Circuits 41 (3), 651–662.
Esposito, M., Newcombe, J., Anaxagoras, T., Allinson, N.M., Wells, K., 2012. Proc. SPIE 8317, 831710.
Finley, S.D., Engel-Stefanini, M.O., Imoukhuede, P., Popel, A.S., 2011. BMC Syst. Biol. 5 (193), 1–20.
Freeman, R., Girsh, J., Ju Jou, A.F., Annie Ho, J., Hug, T., Dernedde, J., Willner, I., 2012. Anal. Chem. 84, 6192–6198.
Gold, L., Janjic, N., 2004. US patent. 6696252.
Huang, H., Ideh, R.C., Gitau, E., Thézénas, M.L., Jallow, M., Ebruke, B., Chimah, O., Oluwalana, C., Karanja, H., Mackenzie, G., Adegbola, R.A., Kwiatkowski, D., Kessler, B.M., Berkley, J.A., Howie, S.R.C., Casals-Pascual, C., 2014. Clin. Infect. Dis. 58 (12), 1707–1715.
Isoshima, T., Isojima, Y., Hakomori, K., Kikuchi, K., Nagai, K., Nakagawa, H., 1995. Rev. Sci. Instrum. 66 (4), 2922–2926.
Janesick, J., 2001. Scientific Charge-Coupled Devices. SPIE Press Belling-ham, WA (volume PM83).
Jelkmann, W., 2001. Clin. Chem. 47 (4), 617–623.
Kaur, H., Yung, L.-Y.L., 2012. Plos One 7 (2), e31196.
Kut, C., Gabhann, F.M., Popel, A., 2007. Br. J. Cancer 97, 978–985.
Lee, H.-S., Kim, K.S., Kim, C.-J., Hahn, S.K., Jo, M.-H., 2009. Biosens. Bioelectron. 24, 1801–1805.
Lenigk, R., Carles, M., Ip, N.Y., Sucher, N.J., 2001. Langmuir 17, 2497–2501.
Li, H., Lopes, N., Moser, S., Sayler, G., Ripp, S., 2012. Biosens. Bioelectron. 33, 299–303.
Li, Z., Han, W., Kozodaev, D., Brokken-Zijp, J.C., de With, G., Thüne, P.C., 2006.

Polymer 47, 1150–1158.
Liu, C., Lei, T., Ino, K., Matsue, T., Tao, N., Li, C.-Z., 2012. Chem. Commun. 48, 10389–10391.
Luchansky, M.S., Bailey, R.C.B., 2012. Anal. Chem. 84, 793–821.
Myers, F.B., Lee, L.P., 2008. Lab Chip 8, 2015–2031.
Nečas, D., Klapetek, P., 2012. Cent. Eur. J. Phys. 10, 181–188.
Palchetti, I., Mascini, M., 2012. Anal. Bioanal. Chem. 402, 3103–3114.
Pasquardini, L., Berneschi, S., Barucci, A., Cosi, F., Dallapiccola, R., Insinna, M., Lunelli, L., Conti, G.N., Pederzolli, C., Salvadori, S., Soria, S., 2013. J. Biophoton. 6 (2), 178–187.
Phaner-Goutorbe, M., Dugas, V., Chevolot, Y., Souteyrand, E., 2011. Mater. Sci. Eng. C 31, 384–390.
Potty, A.S.R., Kourentzi, K., Fang, H., Jackson, G.W., Zhang, X., Legge, G.B., Willson, R. C., 2009. Biopolymers 91 (2), 145–156.
Pro, T., Ferri, A., Gola, A., Serra, N., Tarolli, A., Zorzi, N., Piemonte, C., 2013. IEEE Trans. Nucl. Sci. 60 (3), 2247–2253.
Ramiz, D., Ronen, A., Amit, R., Shimshon, B., Shacahm, D.Y., 2008. Biosens. Bioelectron. 24, 882–887.
Schneider, C.A., Rasband, W.S., Eliceiri, K.W., 2012. Nat. Methods 9 (7), 671–675.
Severi, G., FitzGerald, L.M., Muller, D.C., Pedersen, J., Longano, A., Southey, M.C., Hopper, J.L., English, D.R., Giles, G.G., Mills, J., 2014. Cancer Med. 3 (5), 1266–1274.
Song, S., Wang, L., Li, J., Zhao, J., Fan, C., 2008. Trends Anal. Chem. 27 (2), 108–117.
Wang, S.E., Huang, Y., Hu, K., Tian, J., Zhao, S., 2014. Anal. Methods 6, 62–66.
Zampros, I., Praidou, A., Brazitikos, P., Ekonomidis, P., Androudi, S., 2012. J. Ophthalmol. 2012, 1–12.
Zhang, X., Zhang, H., Xu, S., Sun, Y., 2014. Analyst 139, 133–137.
Zhao, Q., Duan, R., Yuan, J., Quan, Y., Yang, H., Xi, M., 2014. Int. J. Nanomed. 9, 1097–1104.
Zuo, J., Torres, E., 2010. Langmuir 26 (19), 15161–15168.